J. Appl. Comput. Mech., 9(4) (2023) 926-934
DOI: 10.22055/jacm.2023.42310.3906

ISSN: 2383-4536
jacm.scu.ac.ir

Shahid Chamran University of Ahvaz

Journal of Applied and Computational Mechanics

Research Paper

Analysis of Particulate Systems with Numerical Inverse Laplace Transform

Clauderino da Silva Batista[1], Helder Kiyoshi Miyagawa[1], Emanuel Negrão Macêdo[1], João Nazareno Nonato Quaresma[1], Helcio Rangel Barreto Orlande[2]

[1] School of Chemical Engineering, Federal University of Pará, UFPA, Campus do Guamá, Rua Augusto Corrêa, 01, Belém, PA, 66075-110, Brazil, Email: clauderino@ufpa.br (C.S.B); helderkm@ufpa.br (H.K.M.); enegrao@ufpa.br (E.N.M.); quaresma@ufpa.br (J.N.N.Q.)

[2] Laboratory of Transmission and Technology of Heat, Mechanical Engineering Department, Federal University of Rio de Janeiro, Rio de Janeiro, RJ, 21945-970, Brazil, Email: helcio@mecanica.ufrj.br

Received November 12 2022; Revised January 30 2023; Accepted for publication February 24 2023.
Corresponding author: J.N.N. Quaresma (quaresma@ufpa.br)

Abstract. The technique of numerical inversion of the Laplace transform is applied to solve the population balance equation (PBE). The model considers the dispersed phase systems in which nucleation and heterogeneous condensation are present. The studied phenomena model corresponds to a nonlinear integro-partial-differential equation. Test cases are solved considering two different collision mechanisms, the first-order removal mechanism and the effect of simultaneous coagulation and growth. Numerical results are compared with the analytical solution and with the literature. Based on these results, the technique applied in this work demonstrates to be a tool to solve problems in particulate systems, particularly for aerosol modeling where coagulation is the most important inter-particle mechanism affecting the size distribution.

Keywords: Aerosol modeling, Numerical inversion of the Laplace transform, Particle size distribution.

1. Introduction

Dispersed phase systems are the subject of interest in many chemical engineering processes such as fluidized beds [1, 2], droplet dispersions [3], crystallization [4, 5], precipitation [6], liquid-liquid extraction [7, 8], polymerization [9-11], granulation [12, 13], and colloid chemistry [14, 15]. In all such applications, micro-scale processes such as nucleation, particle growth through collisions and coalescence with other particles (coagulation), and agglomeration of particles are present [16, 17]. The modeling approach well suited for systems where nucleation, growth, and aggregation occur is the concept of population balance (PB). In mathematics, the PBE is a strong non-linear equation with the same mathematical structure as Boltzmann's transport equation which corresponds to a nonlinear integro-partial-differential equation and an exact analytical solution is rarely analytically tractable [18, 19] with very few analytical solutions for some ideal cases [20].

Precipitation and crystallization are widely studied problems in modern chemical engineering, which are used to separate and purify solid materials. Several phenomena are involved, such as cooling rate, thermal history, mixing performance, impurities, crystallizer volume/geometry, mixing at various scales, nucleation, crystal growth, aggregation, and breakage [21, 22]. Particle size and size distribution are key to the physical properties of catalysts and other particles or aggregates in nature. Near-monodisperse (≤ ± 15%) if not narrower, approaching monodisperse particle size distributions (PSDs) are highly desirable. Because of this, mechanism-based, rational control of particle size and PSDs is a longstanding goal in nano and other-particle science [23]. Crystallization, which is a widely used solid-liquid separation technique, has three general operation modes, i.e., evaporation of the solvent, cooling down of the solution, and adding antisolvent into the solution. For a practical application, crystal size distribution (CSD) is an important quality index of the prepared particles, which directly influences the product properties such as filtration rate, bioavailability, and dewatering rate [24]. Thus, controlling the CSD of the particles becomes important and challenging work [25].

The population balance equation (PBE) has become a fundamental equation in the study on aerosol dynamical processes, where the most important phenomena are nucleation and heterogeneous condensation, with subsequent coagulation and break-up [26]. Because of the strong dependence of aerosol properties such as scattering, and Brownian coagulation, to predict the aerosol properties, it is desirable to understand in as much detail as possible the inter-particle mechanism affecting the size distribution. The size distribution of an aerosol is described by the number density function of the particles, which is a transient multidimensional equation and can include, volume, surface area, or chemical composition [27], and is governed by a general PBE. Numerical methods must be necessary for simulations of atmospheric aerosol dynamics including turbulence transport and

Published online: March 02 2023

dispersion. However, many analytical solutions for population balance are applied in atmospheric research-related literature [22] and are valuable for the description of the phenomena in more complex particle systems situations [16, 18, 19].

The Laplace transform operation is an excellent alternative to solve the PBE. The PBE is a nonlinear integro-partial-differential equation and the Laplace transform can handle the integral term in PBE directly. Furthermore, the volume domain can be transformed into the Laplace transform domain simplifying the equation. Nevertheless, there is no unique method to perform the numerical inversion of the Laplace transform and the best method must be verified for each studied phenomenon. On this point, the objective of this work is to solve a general model for the size distribution of PBE by applying the Laplace transform technique with numerical Laplace transform inversion to demonstrate the possibility of the numerical inversion for PBE applications enabling future research using the same methodology. An analytical comparison of the present results with solutions presented in the literature for simplified situations is performed to verify the method solution. Moreover, the results obtained in this work are appropriate for characterizing the dynamic behavior of any system of particles in which the phenomena of condensation with subsequent coagulation are present such as crystallization [4, 5] and precipitation [6] processes.

2. Analysis

The general population balance equation of a spatially and chemically homogeneous particulate system considering the mechanisms of agglomeration of the small particles into larger particles (coagulation), condensation and the adding material through the fluid phase (sink or loss of material), Fig. 1, is described in terms of the continuous particle size distribution, $n(\upsilon,t)$ [28-31]:

$$\frac{\partial n(\upsilon,t)}{\partial t} = -\frac{\partial}{\partial \upsilon}\left[I(\upsilon,t)n(\upsilon,t)\right] + \frac{1}{2}\int_0^{\upsilon}\beta(\upsilon-\tilde{\upsilon},\tilde{\upsilon})n(\upsilon-\tilde{\upsilon},t)n(\tilde{\upsilon},t)d\tilde{\upsilon} - n(\upsilon,t)\int_0^{\infty}\beta(\upsilon,\tilde{\upsilon})n(\tilde{\upsilon},t)d\tilde{\upsilon} + S\left[n(\upsilon,t),\upsilon,t\right] \tag{1.a}$$

where t is the time, υ is the particle volume, $I(\upsilon,t)$ is the growth/loss and $I(\upsilon,t)>0$ represents the surface growth rate whereas $I(\upsilon,t)<0$ the evaporation loss rate, S is the nucleation rate including the possible addition of new particles in the system. The integral source term accounts for agglomeration following the continuous counterpart of the Smoluchowski equation where $\beta(\upsilon-\tilde{\upsilon},\tilde{\upsilon})$ represents the coagulation kernel function for particles of volume υ and $\tilde{\upsilon}$. The initial and boundary conditions for Eq. (1.a) are usually given as:

$$n(\upsilon,0) = \frac{N_0}{\upsilon_0}e^{-\upsilon/\upsilon_0}; \quad n(0,t) = 0 \tag{1.b,c}$$

where N_0 and υ_0 are the initial total particle number and the initial total particle volume respectively. The first term on the right side of Eq. (1.a) represents the growth rate of change of a particle size distribution $n(\upsilon,t)$ by mass transfer to individual particles. The second term corresponds to the production of particles by coagulation of the appropriate combinations of smaller particles by the collision of two particles of volume $\beta(\upsilon-\tilde{\upsilon},\tilde{\upsilon})$ and $\tilde{\upsilon}$ to form a particle of volume υ (assuming conservation of volume during coagulation). The third term corresponds to the loss of particles with collisions with all available particles. The last term is the net rate of the addition of fresh particles into the system. Equation (1) provides a wide variety of physical contexts, similar to polymerization, atmospheric dynamics of aerosols, crystallization and precipitation, and biological population dynamics.

2.1 Solution methodology via Laplace transform technique

For solving the mathematical model given by the integro-partial-differential Eq. (1), the Laplace transform with numerical inversion was employed. Therefore, for this purpose, four test cases were considered (Table 1) and compared with the finite element method in the literature [29], namely, i) test-case 1: constant aggregation coefficient $\beta(\upsilon,\tilde{\upsilon})=\beta_0$ and no condensation and source terms $I(\upsilon,t)=S[n(\upsilon,t),\upsilon,t]=0$; ii) test-case 2: linear aggregation coefficient $\beta(\upsilon,\tilde{\upsilon})=\beta_1(\upsilon+\tilde{\upsilon})$ and no condensation and source terms $I(\upsilon,t)=S[n(\upsilon,t),\upsilon,t]=0$, iii) test-case 3: constant aggregation coefficient $\beta(\upsilon-\tilde{\upsilon},\tilde{\upsilon})=\beta_0$ with linear growth rate $I(\upsilon,t)=\sigma\upsilon$ and no source terms, and iv) test-case 4: linear aggregation coefficient $\beta(\upsilon,\tilde{\upsilon})=\beta_1(\upsilon+\tilde{\upsilon})$ no condensation and particle removal rate $S[n(\upsilon,t),\upsilon,t]=-R_0 n(\upsilon,t)$.

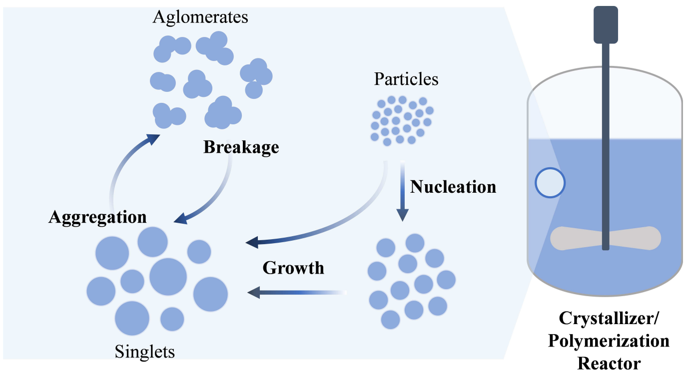

Fig. 1. Schematic configuration of the considered structure/system.

Table 1. Test Cases for the studied phenomena.

Test Case	Aggregation $\beta(\upsilon,\tilde{\upsilon})$	Condensation $I(\upsilon,t)$	Source Term $S[n(\upsilon,t),\upsilon,t]$
1	β_0	-	-
2	$\beta_1(\upsilon+\tilde{\upsilon})$	-	-
3	β_0	$\sigma\upsilon$	-
4	$\beta_1(\upsilon+\tilde{\upsilon})$	-	$-R_0 n(\upsilon,t)$

2.1.1 Test-case 1

The Laplace transform procedure of Eq. (1.a), to remove the independent variable υ, for the test-case 1 is now established as follows:

$$\mathcal{L}\left[\frac{\partial n(\upsilon,t)}{\partial t}\right]=\frac{\partial \bar{n}(s,t)}{\partial t};\ \mathcal{L}\left[\frac{\beta_0}{2}\int_0^{\upsilon} n(\upsilon-\tilde{\upsilon},t)n(\tilde{\upsilon},t)d\tilde{\upsilon}\right]=\frac{\beta_0}{2}\bar{n}^2(s,t);\ \mathcal{L}\left[\beta_0 n(\upsilon,t)\int_0^{\infty} n(\tilde{\upsilon},t)d\tilde{\upsilon}\right]=\beta_0 M_0(t)\bar{n}(s,t) \tag{2.a-c}$$

where, $\bar{n}(s,t)=\mathcal{L}[n(\upsilon,t)]$. Therefore, the transformed differential equation for this case, from the results of Eqs. (2), together with the transformed initial condition, are written as:

$$\frac{\partial \bar{n}(s,t)}{\partial t}+\beta_0 M_0(t)\bar{n}(s,t)=\frac{\beta_0}{2}\bar{n}^2(s,t) \tag{3.a}$$

$$\bar{n}(s,0)=\frac{(N_0/\upsilon_0)}{s+(1/\upsilon_0)} \tag{3.b}$$

The zeroth order moment $M_0(t)$ that appears in Eq. (3.a) is obtained from its usual definition, and in this case is given by [32]:

$$M_0(t)=\int_0^{\infty} n(\upsilon,t)d\upsilon=\frac{2N_0}{2+\beta_0 N_0 t} \tag{3.c}$$

Equations (3) are readily analytically solved, resulting:

$$\bar{n}(s,t)=\frac{4(N_0/\upsilon_0)}{(2+\beta_0 N_0 t)^2\{s+2/[(2+\beta_0 N_0 t)\upsilon_0]\}} \tag{4}$$

Applying the inverse Laplace transform in Eq. (4), one obtains:

$$n(\upsilon,t)=\mathcal{L}^{-1}[\bar{n}(s,t)]=\frac{4(N_0/\upsilon_0)}{(2+\beta_0 N_0 t)^2}\mathcal{L}^{-1}\left[\frac{1}{\{s+2/[(2+\beta_0 N_0 t)\upsilon_0]\}}\right]=\frac{4(N_0/\upsilon_0)}{(2+\beta_0 N_0 t)^2}\exp\left[-\frac{2}{(2+\beta_0 N_0 t)}\frac{\upsilon}{\upsilon_0}\right] \tag{5}$$

Assuming spherical particles, the volume distribution density is now related to its diameter distribution density through:

$$n_D(D,t)=n(\upsilon,t)\frac{d\upsilon}{dD}=\frac{\pi D^2}{2}n(\upsilon,t) \tag{6}$$

Therefore, introducing Eq. (5) into Eq. (6), it results in:

$$n_D(D,t)=\frac{12(N_0/D_0)(D/D_0)^2}{(2+\beta_0 N_0 t)^2}\exp\left[-\frac{2}{(2+\beta_0 N_0 t)}\left(\frac{D}{D_0}\right)^3\right] \tag{7}$$

2.1.2 Test-case 2

Similarly, the Laplace transform procedure of Eq. (1.a) for the test-case 2 is done, to obtain:

$$\begin{gathered}\mathcal{L}\left[\frac{\partial n(\upsilon,t)}{\partial t}\right]=\frac{\partial \bar{n}(s,t)}{\partial t};\quad \mathcal{L}\left[\frac{\beta_1}{2}\int_0^{\upsilon}\upsilon n(\upsilon-\tilde{\upsilon},t)n(\tilde{\upsilon},t)d\tilde{\upsilon}\right]=-\beta_1\bar{n}(s,t)\frac{\partial \bar{n}(s,t)}{\partial s};\\ \mathcal{L}\left[\beta_1 n(\upsilon,t)\int_0^{\infty}(\upsilon+\tilde{\upsilon})n(\tilde{\upsilon},t)d\tilde{\upsilon}\right]=-\beta_1 M_0(t)\frac{\partial \bar{n}(s,t)}{\partial s}+\beta_1 M_1(t)\bar{n}(s,t)\end{gathered} \tag{8.a-c}$$

The transformed differential equation for this case is given from Eqs. (8), in the form:

$$\frac{\partial \bar{n}(s,t)}{\partial t}+\beta_1[\bar{n}(s,t)-M_0(t)]\frac{\partial \bar{n}(s,t)}{\partial s}=-\beta_1 M_1(t)\bar{n}(s,t) \tag{9.a}$$

$$\bar{n}(s,0)=\frac{(N_0/\upsilon_0)}{s+(1/\upsilon_0)} \tag{9.b}$$

where, the zeroth and first-order moments, $M_0(t)$ and $M_1(t)$, respectively, in Eq. (9.a) are obtained as [32]:

$$M_0(t)=\int_0^{\infty} n(\upsilon,t)d\upsilon=N_0\exp(-\beta_1\upsilon_0 N_0 t);\quad M_1(t)=\int_0^{\infty}\upsilon n(\upsilon,t)d\upsilon=\upsilon_0 N_0 \tag{9.c,d}$$

Equation (9.a) is a hyperbolic-type differential equation and is analytically solved through the method of characteristics, to yield:

$$\bar{n}(s,t)=-\frac{\upsilon_0 N_0\exp(-\beta_1\upsilon_0 N_0 t)}{2[1-\exp(-\beta_1\upsilon_0 N_0 t)]}\left\{\sqrt{\left[s+\frac{2-\exp(-\beta_1\upsilon_0 N_0 t)}{\upsilon_0}\right]^2-\left[\frac{2}{\upsilon_0}\sqrt{[1-\exp(-\beta_1\upsilon_0 N_0 t)]}\right]^2}-\left[s+\frac{2-\exp(-\beta_1\upsilon_0 N_0 t)}{\upsilon_0}\right]\right\} \tag{10}$$

The inverse Laplace transform of Eq. (10) is given by [32]:

$$n(v,t)=\mathcal{L}^{-1}[\bar{n}(s,t)]=-\frac{v_0N_0\exp(-\beta_1v_0N_0t)}{2[1-\exp(-\beta_1v_0N_0t)]}\mathcal{L}^{-1}\left[\sqrt{\left[s+\frac{2-\exp(-\beta_1v_0N_0t)}{v_0}\right]^2-\left[\frac{2}{v_0}\sqrt{[1-\exp(-\beta_1v_0N_0t)]}\right]^2}-\left[s+\frac{2-\exp(-\beta_1v_0N_0t)}{v_0}\right]\right]=\frac{N_0\exp(-\beta_1v_0N_0t)}{v\sqrt{[1-\exp(-\beta_1v_0N_0t)]}}\exp\left\{-[2-\exp(-\beta_1v_0N_0t)]\frac{v}{v_0}\right\}I_1\left[2\sqrt{[1-\exp(-\beta_1v_0N_0t)]}\frac{v}{v_0}\right] \tag{11}$$

Applying Eq. (6) to Eq. (11), the diameter distribution density is obtained as:

$$n_D(D,t)=\frac{3(N_0/D_0)\exp(-\beta_1v_0N_0t)}{(D/D_0)\sqrt{[1-\exp(-\beta_1v_0N_0t)]}}\exp\left\{-[2-\exp(-\beta_1v_0N_0t)]\left(\frac{D}{D_0}\right)^3\right\}I_1\left[2\sqrt{[1-\exp(-\beta_1v_0N_0t)]}\left(\frac{D}{D_0}\right)^3\right] \tag{12}$$

2.1.3 Test-case 3

For this case, the only difference, concerning the test-case 1, is the Laplace transform of the first term on the right side of Eq. (1.a), which is given as follows:

$$\mathcal{L}\left[\frac{\partial[\sigma v n(v,t)]}{\partial v}\right]=-\sigma s\frac{\partial\bar{n}(s,t)}{\partial s} \tag{13}$$

Therefore, the transformed differential equation for this test-case 3 is obtained from Eqs. (2), in conjunction with Eq. (13), to yield:

$$\frac{\partial\bar{n}(s,t)}{\partial t}-\sigma s\frac{\partial\bar{n}(s,t)}{\partial s}=\frac{\beta_0}{2}\bar{n}^2(s,t)-\beta_0M_0(t)\bar{n}(s,t) \tag{14.a}$$

$$\bar{n}(s,0)=\frac{(N_0/v_0)}{s+(1/v_0)} \tag{14.b}$$

where the zeroth order moment $M_0(t)$ is the same as given by Eq. (3.c). Equation (14.a) is also analytically solved through the method of characteristics, to yield:

$$\bar{n}(s,t)=\frac{4(N_0/v_0)e^{-\sigma t}}{(2+\beta_0N_0t)^2\{s+2e^{-\sigma t}/[(2+\beta_0N_0t)v_0]\}} \tag{15}$$

The inverse Laplace transform of Eq. (15) is:

$$n(v,t)=\mathcal{L}^{-1}[\bar{n}(s,t)]=\frac{4(N_0/v_0)e^{-\sigma t}}{(2+\beta_0N_0t)^2}\mathcal{L}^{-1}\left[\frac{1}{\{s+2e^{-\sigma t}/[(2+\beta_0N_0t)v_0]\}}\right]=\frac{4(N_0/v_0)}{(2+\beta_0N_0t)^2}\exp\left[-\frac{2e^{-\sigma t}}{(2+\beta_0N_0t)}\frac{v}{v_0}-\sigma t\right] \tag{16}$$

In terms of diameter distribution density by applying Eq. (6) into Eq. (16), one has:

$$n_D(D,t)=\frac{12(N_0/D_0)(D/D_0)^2}{(2+\beta_0N_0t)^2}\exp\left[-\frac{2e^{-\sigma t}}{(2+\beta_0N_0t)}\left(\frac{D}{D_0}\right)^3-\sigma t\right] \tag{17}$$

2.1.4 Test-case 4

For this case, the only difference, concerning the test-case 2, is the Laplace transform of the last term on the right side of Eq. (1.a), which is given as follows:

$$\mathcal{L}[R_0n(v,t)]=R_0\bar{n}(s,t) \tag{18}$$

Therefore, the transformed differential equation for this test-case 4 is obtained from Eqs. (9), in conjunction with Eq. (18), to yield:

$$\frac{\partial\bar{n}(s,t)}{\partial t}-\beta_1\left[M_0(t)-(\bar{n}(s,t))\right]\frac{\partial\bar{n}(s,t)}{\partial s}=-(\beta_1M_1(t)+R_0)\bar{n}(s,t) \tag{19.a}$$

$$\bar{n}(s,0)=\frac{(N_0/v_0)}{s+(1/v_0)} \tag{19.b}$$

where, the zeroth and first-order moments, $M_0(t)$ and $M_1(t)$, respectively, in Eq. (19.a) are shown below:

$$M_0(t)=\int_0^\infty n(v,t)dv=N_0\exp\left(\frac{\beta_1v_0N_0\left(\exp(-R_0t)-1\right)}{R_0}-R_0t\right);\qquad M_1(t)=\int_0^\infty vn(v,t)dv=v_0N_0\exp(-R_0t) \tag{20.a,b}$$

Equation (19.a) is also analytically solved through the method of characteristics, to yield:

$$\bar{n}(S,\tilde{T})=-\frac{1}{2\tilde{g}v_0}\tilde{T}N_0\exp\left(\frac{\tilde{T}-1}{\theta}\right)\left\{\sqrt{S^2-A^2}-S\right\} \tag{21}$$

Table 2. Results of comparison by both analytical and numerical Laplace transform inversion against the literature [29].

Test Case	τ = 0.25	τ = 1.0	τ = 2.0	τ = 10.0	τ = 20.0
1	0.00010	0.00358	0.00643	0.00684	0.00066
2	0.00578	0.02677	0.03443	-	-
3	0.00145	0.00248	0.00397	-	-
4	0.00201	0.00286	0.00757	-	-

where $\theta = R_0 / N_0 \upsilon_0 \beta_1$, $\tau = N_0 \beta_0 \upsilon_0 t$, $\tilde{T} = \exp(-\theta\tau)$, $\tilde{g} = 1 - \exp\left[\left(\tilde{T} - 1\right)/\theta\right]$, $S = s + (1+\tilde{g})\upsilon_0$ and $A = 2\upsilon_0\sqrt{\tilde{g}}$. The inverse Laplace transform of Eq. (21) is:

$$n(\upsilon, T) = -\frac{\tilde{T}N_0}{2\tilde{g}\upsilon_0}\exp\left(\frac{\tilde{T}-1}{\theta}\right)\exp\left[-(1+\tilde{g})\upsilon_0\upsilon\right]\mathcal{L}^{-1}\left[\sqrt{S^2 - A^2} - S\right] \tag{22}$$

In terms of diameter distribution density by applying Eq. (6) into Eq. (16), one has:

$$n(\upsilon, T) = -\frac{\tilde{T}N_0}{\upsilon\sqrt{\tilde{g}}}\exp\left(\frac{\tilde{T}-1}{\theta}\right)\exp\left[-(1+\tilde{g})\upsilon_0\upsilon\right]I_1(2\sqrt{\tilde{g}}\upsilon\upsilon_0) \tag{23}$$

2.2 The numerical inverse Laplace Transforms

The Laplace transform has also the advantage that it solves problems directly, initial value problems without determining first a general solution and nonhomogeneous differential equations without solving first the corresponding homogeneous equations [33]. The Laplace transform of $f(t)$ given by $F(s) = \int_0^\infty f(t)e^{-st}dt$ is a highly stable operation since variations in $f(t)$ are averaged out in integration. Furthermore, the Laplace transform kernel, e^{-st}, converges asymptotically to zero when t tends to infinity, unless s is small, which implies that large variation on $f(t)$ indicates small $F(s)$ changes. However, difficulties may be encountered in the inversion step of the transformation because the inversion may not be possible through the usual techniques and the inverse Laplace transform is generally done numerically. There are over 100 methods available for the numerical inversion of Laplace transforms [34] based on the approximation of the inversion complex integral, PostWidder inversion formula, and methods based on the deformation of the contour of the Bromwich inversion integral [35].

Equations (4), (10), (15), and (21) are all non-linear in the s-variable. Particularly, for these test cases, it was possible to perform the inverse Laplace transform. However, difficulties may be found while using the Laplace transform to solve a differential equation in the inversion of the solutions from the Laplace domain to the time domain [36], and where the inverse transform cannot be determined analytically.

Alternatively, aiming at more general cases, in the present work, Eqs. (4), (10), (15), and (21) are numerically inverted through of the subroutine DINLAP from [37] at each time and spatial position of interest with a required tolerance of 10^{-4}. The DINLAP is an optimized subroutine for high-performance computation from the thoroughly-tested IMSL Fortran Library and computes the inverse Laplace transform of a complex-valued function. The computation of the inverse Laplace transform is based on applying the epsilon algorithm to the complex Fourier series obtained as a discrete approximation to the inversion integral [37]. Given a complex-valued transform F(s), the trapezoidal rule gives the approximation to the inverse transform.

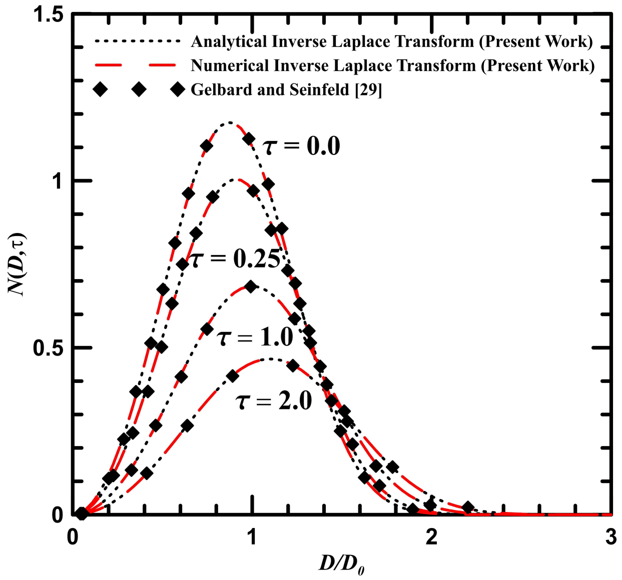

Fig. 2. Comparison of $N(D,\tau)$ distribution for pure coagulation with constant kernel (test-case 1).

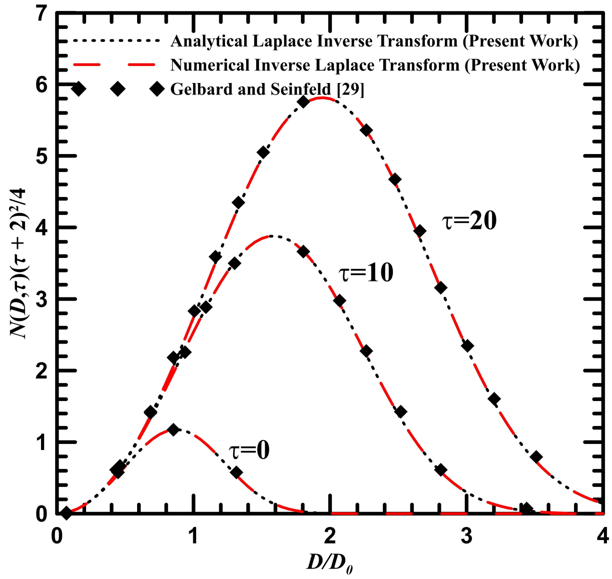

Fig. 3. Comparison of $N(D,\tau)$ distribution for pure coagulation with constant kernel and ratio (D/D_0) in the range [0,4] (test-case 1).

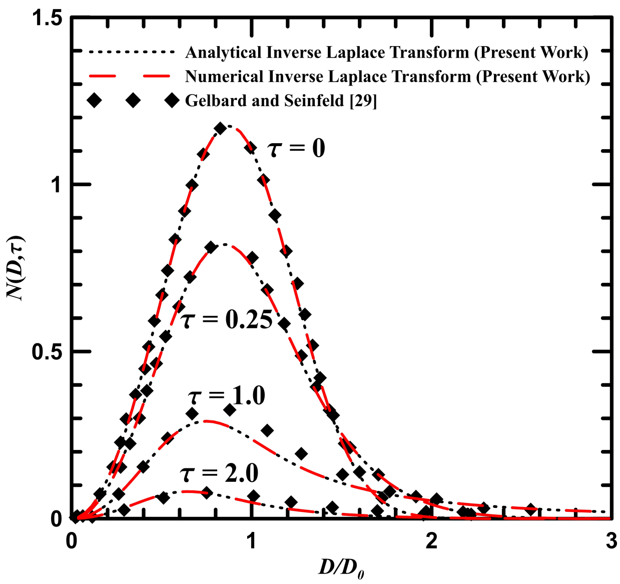

Fig. 4. Comparison of $N(D,\tau)$ distribution for pure coagulation with varying kernel (test-case 2).

3. Results and Discussions

The results of the numerical inversion for the four test cases were obtained in terms of diameter distribution. The codes were implemented in Fortran 90/95 programming language, which was run on a Pentium IV 1.70 GHz computer. For the numerical inversion of Eqs. (4), (10), (15), and (21), the subroutine DINLAP from the [37] was used with a tolerance of 10^{-4}.

The comparison of results in the present work by both analytical and numerical Laplace transform inversion are compared against the results reported in the literature [29] for the solution of Eq. (1.a) by finite element method considering two different collisions mechanisms, first-order removal mechanism and the effect of simultaneous coagulation and growth, here referred to as test-case 1, 2, 3, and 4. The summary of the results can be observed in Table 2 in terms of mean absolute error. In Table 2 the comparison of numerical Laplace inversion against analytical Laplace transform inversion is suppressed since the calculated absolute error is less than 10^{-7}.

The simplest form of Eq. (1.a) is considering the absence of growth and sources with constant collision mechanisms (case 1). Figure 2 shows the numerical inversion and exact results for the diameter density for the test-case 1 (pure coagulation with the constant kernel), using equally space elements in the range [0,3] of the ratio (D/D_0), for the dimensionless times $(\tau = \beta_0 N_0 t)$, $\tau = 0$, 0.25, 1.0 and 2.0. An excellent agreement between the numerical inversion and exact solution was obtained, as well as with the results of [29]. Here, this is related to the diameter distribution in the dimensionless form: $N(D,\tau) = D_0 n_D(D,\tau)/N_0$. The precipitation and growth of particles are the result of several mechanisms, nucleation, molecular growth, and secondary processes such as aggregation and breakage. The phenomena of nucleation and growth are competitive, both consume the solute molecules and therefore the particle size is the result of this competition over time. In Fig. 2 it is noted that at time zero, the system precipitates many particles, increasing the population density of these particles. As time increased the phenomena of nucleation and growth happen simultaneously consuming the excess of these particles, providing their growth, and decreasing the density of the precipitated particles.

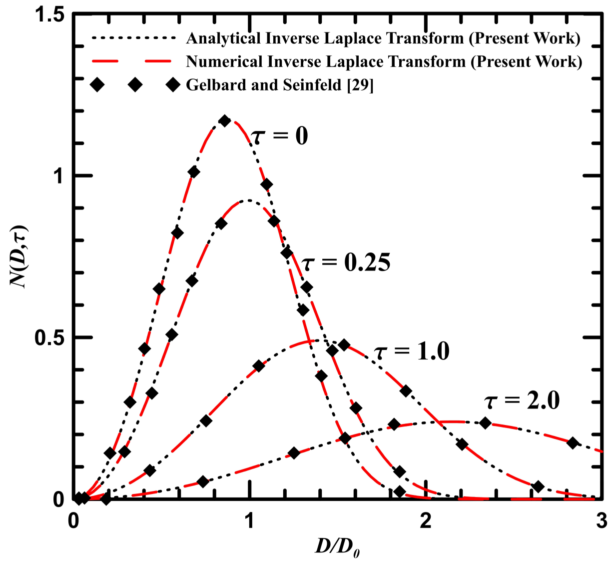

Fig. 5. Comparison of $N(D,\tau)$ distribution for both coagulation and particle growth with constant kernel (test-case 3).

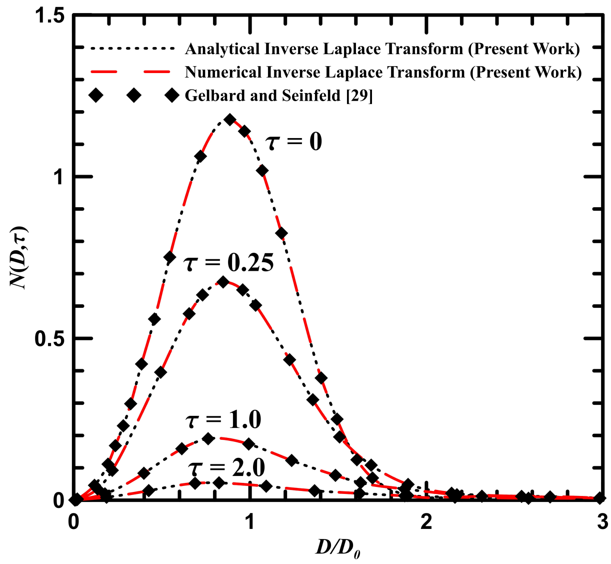

Fig. 6. Comparison of $N(D,\tau)$ distribution for coagulation with varying kernel and removal rate (test-case 4).

Figure 3, using equally space elements in the range [0,4] of the ratio (D/D_0), shows a similar analysis as for Fig. 2, however, to demonstrate the performance of both techniques for long times (τ = 0, 10.0, and 20.0), the distribution $N(D,\tau)$ is multiplied by the term $(\tau+2)^2/4$. Also, an excellent agreement among the results is verified. In contrast to Fig. 2, in Fig. 3, considering long times, most of the molecules are already nucleated and the growth mechanism is dominant increasing both the density of the precipitated particles and the ratio (D/D_0).

Figure 4 shows a comparison of the $N(D,\tau)$ distribution for pure coagulation with varying kernel (test-case 2), also using equally space elements in the range [0,3] of the ratio (D/D_0), for the dimensionless times using equally space elements in the range [0,3] of the ratio (D/D_0), for the dimensionless times ($\tau=\beta_0 \upsilon_0 N_0 t$), τ = 0, 0.25, 1.0 and 2.0. Once again, the three sets of results are in excellent agreement, which emphasizes the ability of the Laplace transform with numerical inversion in handling such types of problems. Compared to Fig. 2, in Fig. 4 the particle sizes are shifted faster than in case 1 due to the linear collision mechanism whereas in case 1 the collision is a constant.

Figure 5 shows the numerical inversion and exact results for the comparison of the $N(D,\tau)$ distribution for both coagulation and particle growth with constant kernel (test-case 3), using equally space elements in the range [0,3] of the ratio (D/D_0), for the dimensionless times ($\tau=\beta_0 N_0 t$), τ = 0, 0.25, 1.0 and 2.0. As observed throughout the analysis an excellent agreement is verified among the sets of results. Compared to Fig. 2, in Fig. 5 the particle sizes are shifted faster than in case 1 due to the linear growth rate. Moreover, the linear growth rate condition causes the centrality of the density to be shifted as time is increased.

Figure 6 shows the comparison of $N(D,\tau)$ distribution for coagulation with varying kernel and removal rate (test-case 4), also using equally space elements in the range [0,3] of the ratio (D/D_0), for the dimensionless times ($\tau=\beta_0 \upsilon_0 N_0 t$), τ = 0, 0.25, 1.0 and 2.0. Note that, an excellent agreement among the results is verified. Compared to Fig. 4, in Fig. 6 the particle size distributions are flattened due to the imposed particle removal rate.

4. Conclusion

The numerical inversion of the Laplace transform was successfully applied for the solution of the population balance equation. The studied cases considered different collision mechanisms, removal mechanisms, and growth. Because there is no universal method of numerical inversion that works well for all problems, the comparison of the numerical inversion in cases where the analytic inverse transform is known enables a more rational choice of the method to be used. The FORTRAN subroutine DINLAP performed the numerical inversion of the Laplace transform. The results generated were compared with data produced by the analytical solution, which have an excellent agreement. Thus, the method demonstrated to be an alternative tool for handling problems mathematically described by integro-differential equations, particularly for particulate systems. Considering the results presented in this work the population balance equation can also be solved using the Laplace transform technique with numerical inversion in problems where the same micro-scale processes. In such processes nucleation, growth, and agglomeration of particles can be present as in precipitation and crystallization processes

Author Contributions

C. da Silva Batista planned the scheme, initiated the project, and developed the code; H.K. Miyagawa performed the mathematical simulation and validated the results; E.N. Macêdo suggested the methodology for conducting the project; J.N.N. Quaresma developed the mathematical modeling and examined the theory validation. H.R.B. Orlande developed the code and conducted the analysis. The manuscript was written through the contribution of all authors. All authors discussed the results, reviewed, and approved the final version of the manuscript.

Acknowledgments

Not applicable.

Conflict of Interest

The authors declared no potential conflicts of interest concerning the research, authorship, and publication of this article.

Funding

The authors received no financial support for the research, authorship, and publication of this article.

Data Availability Statements

The datasets generated and/or analyzed during the current study are available from the corresponding author on reasonable request.

Nomenclature

D	Particle diameter [μm]
D_0	Initial particle diameter [μm]
$I_v(v,t)$	Rate of change of volume by mass transfer between particles and fluid
K_t	Perturbation kernel
$n(v,t)$	Size distribution density function [μm^{-3}.cm^{-3}]
$n(D,t)$	Size distribution density function as a function of diameter [μm^{-1}.cm^{-1}]
$N(D,\tau)$	Dimensionless size distribution density function
N_0	Total number of particle at $t = 0$ [cm^{-3}]
R_0	Removal Rate [cm³.s^{-1}]
s	Laplace transform domain
S	Net rate of addition or removal of particles in the system [cm³.s^{-1}]
v	Particle volume [cm³]
w	Importance weights

Greek Letters

β	Coagulation coefficient
β_0	Constant aggregation coefficient [cm³.s^{-1}]
β_1	Linear aggregation coefficient [cm³.s^{-1}]
τ	Dimensionless time

References

[1] Amini, H., He, X., Tseng, Y.-C., Kucuk, G., Schwabe, R., Schultz, L., Maus, M., Schroder, D., Rajniak, P., Bilgili, E., A semi-theoretical model for simulating the temporal evolution of moisturetemperature during industrial fluidized bed granulation, *European Journal of Pharmaceutics and Biopharmaceutics*, 151, 2020, 137–52.
[2] Kaur G., Singh M., Kumar J., De Beer T., Nopens I., Mathematical modelling and simulation of a spray fluidized bed granulator, *Processes*, 6, 2018, 195.
[3] Gong, H., Yang, Y., Yu, B., Luo, X., Peng, Y., Jiang, Y., Coalescence characteristics of droplets dispersed in oil subjected to electric and centrifugal fields, *Colloids and Surfaces A: Physicochemical and Engineering Aspects*, 648, 2022, 129398.
[4] Costa, C.B.B., Maciel, M.R.W., Filho, R.M., Considerations on the crystallization modeling: population balance solution, *Computers & Chemical Engineering*, 31, 2007, 206–18.
[5] Farias, L.F., de Souza, J.A., Braatz, R.D., da Rosa, C.A., Coupling of the population balance equation into a two-phase model for the simulation of combined cooling and antisolvent crystallization using openfoam Comput, *Chemical Engineering*, 123, 2019, 246–56.
[6] Vasquez, C.C.R., Lebaz, N., Ramière, I., Lalleman, S., Mangin, D., Bertrand, M., Fixed point convergence and acceleration for steady state population balance modelling of precipitation processes: Application to neodymium oxalate, *Chemical Engineering Research and Design,* 177, 2022, 767–777.
[7] Maluta, F., Buffo, A., Marchisio, D., Montante, G., Paglianti, A., Vanni, M., Numerical and Experimental Analysis of the Daughter Distribution in Liquid-Liquid Stirred Tank, *Chemical Engineering & Technology*, 44(11), 2021, 1994–2001.
[8] Rajamani, K., Pate, W.T., Kinneberg, D.J., Time-driven and event-driven Monte Carlo simulations of liquid–liquid dispersions: a comparison, *Industrial & Engineering Chemistry Fundamentals*, 25, 1986, 746.
[9] Kiparissides, C., Challenges in particulate polymerization reactor modeling and optimization: a population balance perspective, *Journal of Process Control*, 16, 2006, 205–24.

[10] Kirse, C., Briesen, H., Numerical solution of mixed continuous-discrete population balance models for depolymerization of branched polymers, *Computers & Chemical Engineering*, 73, 2015, 154–71.
[11] Kotoulas, C., Kiparissides, C., A generalized population balance model for the prediction of particle size distribution in suspension polymerization reactors, *Chemical Engineering Science*, 61, 2006, 332–46.
[12] Barrasso, D., Eppinger, T., Pereira, F.E., Aglave, R., Debus, K., Bermingham, S.K., Ramachandran, R., A multi-scale, mechanistic model of a wet granulation process using a novel bi-directional PBM-DEM coupling algorithm, *Chemical Engineering Science*, 123, 2015, 500–13.
[13] Barrasso, D., Walia, S., Ramachandran, R., Multi-component population balance modeling of continuous granulation processes: a parametric study and comparison with experimental trends, *Powder Technology*, 241, 2013, 85–97.
[14] Kostoglou, M., Extended cell average technique for the solution of coagulation equation, *Journal of Colloid and Interface Science*, 306, 2007, 72–81.
[15] Tandon, P., Rosner, D.E., Monte Carlo simulation of particle aggregation and simultaneous restructuring, *Journal of Colloid and Interface Science*, 213, 1999, 273–86.
[16] Ramabhadran, T.E., Peterson, T.W., Seinfeld, J.H., Dynamics of Aerosol Coagulation and Condensation, *AIChE Journal*, 22, 1976, 840-851.
[17] Gerstlauer, A., Gahn, C., Zhou, H., Rauls, M., Schreiber, M., Application of population balances in the chemical industry - current status and future needs, *Chemical Engineering Science*, 61, 2006, 205–217.
[18] Litster, J.D., Smit, D.J., Hounslow, M.J., Adjustable Discretized Population Balance for Growth and Aggregation, *AIChE Journal*, 41, 1995, 591-603.
[19] Yua, M., Lin, J., Cao, J., Seipenbuschc, M., An analytical solution for the population balance equation using a moment method, *Particuology*, 18, 2015, 194–200.
[20] Bertin, D., Cotabarren, I., Piña, J., Bucalá, V., Population balance discretization for growth, attrition, aggregation, breakage and nucleation, *Computers and Chemical Engineering*, 84, 2016, 132–150.
[21] Marchisio, D.L., Pikturna, J.T., Fox, R.O., Vigil, R.D., Barresi, A.A., Quadrature Method of Moments for Population-Balance Equations, *AIChE Journal*, 49, 2003, 1266-1276.
[22] Omar, H.M., Rohani, S., Crystal Population Balance Formulation and Solution Methods: A Review, *Crystal Growth & Design*, 17, 2017, 4028–4041.
[23] Handwerk, D.R., Particle Size Distributions via Mechanism-Enabled Population Balance Modeling, *The Journal of Physical Chemistry C*, 124(8), 2020, 4852-4880.
[24] Ghadipasha, N., Romagnoli, J.A., Tronci, S., Baratti, R., On-line control of crystal properties in nonisothermal antisolvent crystallization, *AIChE Journal*, 61, 2015, 2188–2201.
[25] Wu, B., Li, J., Li, C., He, J., Luo, P., Antisolvent crystallization intensified by a jet crystallizer and a method for investigating crystallization kinetics, *Chemical Engineering Science*, 211, 2020, 115259.
[26] Frederix, E.M.A., Stanic, M., Kuczaj, A.K., Nordlund, Geurts, M.B.J., Characteristics-based sectional modeling of aerosol nucleation and condensation, *Journal of Computational Physics*, 326, 2016, 499–515.
[27] Nguyena, T.T., Laurenta, F., Foxa, R.O., Massot, M., Solution of population balance equations in applications with fine particles, *Mathematical Modeling and Numerical Schemes*, 325, 2016, 129-156.
[28] Peterson, T.W., Gelbard, F., Seinfeld, J.H., Dynamics of Source-Reinforced, Coagulating, and Condensing Aerosols, *Journal of Colloid and Interface Science*, 63, 1978, 426-445.
[29] Gelbard, F., Seinfeld, J.H., Numerical Solution of the Dynamic Equation for Particulate Systems, *Journal of Computational Physics*, 28, 1978, 357-375.
[30] Drake, R.L., *Topics in Current Aerosol Research*, Hidy, G. and Brock, J., Eds., Pergamon, Oxford, 1972.
[31] Seinfeld, J.H., Pandis, S.N., *Atmospheric chemistry and physics: from air pollution to climate change*, Wiley-Interscience, New York, 2006.
[32] Abramowitz, M., Stegun, I.A., *Handbook of Mathematical Functions with Formulas, Graphs, and Mathematical Tables*, Dover Publications, New York, 1972.
[33] Hussanan, A., Khan, I., Shafie, S., An Exact Analysis of Heat and Mass Transfer Past a Vertical Plate with Newtonian Heating, *Journal of Applied Mathematics,* 2013, 2013, 1-9
[34] Abate, J., Valkó, P.P., Multi-precision Laplace transform inversion, *International Journal for Numerical Methods in Engineering*, 60(5), 2004, 979-993
[35] Krylov, V.I., Skoblya, N.S., *Handbook of Numerical Inversion of Laplace Transforms*, Israel Program for Scientific Translation, Jerusalem, 1969.
[36] Pilatti, C., Rodriguez, B.D., do, A., Prolo Filho, J.F., Performance Analysis of Stehfest and Power Series Expansion Methods for Solution to Diffusive and Advective Transport Problems, *Defect and Diffusion Forum*, 396, 2019, 99-108.
[37] IMSL Library, Math/Lib, Houston, TX, 1991.

ORCID iD

Clauderino da Silva Batista https://orcid.org/0000-0002-8506-4534
Helder Kiyoshi Miyagawa https://orcid.org/0000-0001-9346-4696
Emanuel Negrão Macêdo https://orcid.org/0000-0002-4652-8316
João Nazareno Nonato Quaresma https://orcid.org/0000-0001-9365-7498
Helcio Rangel Barreto Orlande https://orcid.org/0000-0002-3511-322X

How to cite this article: da Silva Batista C., Miyagawa H.K., Macêdo E.N., Quaresma J.N.N., Orlande H.R.B. Analysis of Particulate Systems with Numerical Inverse Laplace Transform, *J. Appl. Comput. Mech.*, 9(4), 2023, 926–934. https://doi.org/10.22055/jacm.2023.42310.3906